Surface Modification of Carbon Nanofibers Via Deposition of an Ultrathin Coating of Plasma-Polymerized Poly(acrylic acid) and Its Effect on the Properties of Polyamide 6/CNF Nanocomposites

E. Hernández-Hernández, M. G. Neira-Velázquez, J. Mendez-Nonell, L. F. Ramos-deValle

Centro de Investigación en Química Aplicada (CIQA), Boulevard Enrique Reyna # 140, Saltillo, Coahuila 25253, México

Received 26 May 2008; accepted 21 December 2008
DOI 10.1002/app.29932
Published online 6 March 2009 in Wiley InterScience (www.interscience.wiley.com).

ABSTRACT: Carbon nanofibers (CNFs) were coated with an ultrathin layer of poly(acrylic acid) (PAA) via plasma polymerization. The effect of the plasma reactor parameters on the extent of the CNF modification was studied. SEM micrographs showed that surface roughness increased with the plasma treatment. The thickness of the ultrathin PAA layer deposited on the CNF was determined by STEM to be ca. 8 nm. Untreated and treated CNF were melt-mixed with polyamide 6 (PA6) in a Brabender mixing chamber to obtain PA6/CNF nanocomposites. The effect of the plasma treatment on the dispersion and compatibility was examined and found to improve markedly. Fractured tensile specimens showed that the CNF seemed to be completely embedded in the polymer matrix, indicating high compatibility between the PA6 and the PAA-coated CNF. Tensile stress and tensile modulus of PA6 nanocomposites with treated CNF were found to increase by 30 and 48%, respectively, when compared with those with untreated CNF. However, the increase in tensile stress and modulus with respect to pure PA6 was 52 and 88%, respectively. Finally, XRD showed that the CNF induce the formation of the α (alpha)-crystalline phase in PA6. © 2009 Wiley Periodicals, Inc. J Appl Polym Sci 112: 3510–3518, 2009

Key words: carbon nanofibers; polyamide 6 (nylon 6); plasma polymerization; polymer nanocomposites

INTRODUCTION

The success of nanoparticles as reinforcing agents in polymer composites is due to their intrinsic mechanical properties. A requisite for these nanoparticles to be effective is their compatibility toward the polymer matrix. Nonetheless, incompatibility is the most common issue when dealing with polymer–nanoparticle composites. In this respect, a great effort has been dedicated to study the effect of modifying with specific functional groups, either the nanoparticles[1–4] or the polymer matrix[5,6] to improve compatibility between them. Another line of study is the use of a third substance, which would act as a compatibilizer.[7–10]

Also, compatibility, another important factor that directly affects the properties of the polymeric nanocomposite is the degree of dispersion of the nanoparticles. In this respect, the positive effect of shear during mixing has been demonstrated in attaining optimum levels of dispersion.[11]

One of the methods that can be used to modify the nanoparticles is the plasma technique. This is a relatively simple, rapid, and dry method that has been used to modify the surface of different substrates. Although it was originally implemented to modify the surface of polymeric substrates,[12,13] this technique has been successfully used during the last decade for the surface modification of different filler particles, such as zinc, iron, and aluminum oxide nanoparticles, and carbon nanofibers (CNFs) and carbon nanotubes (CNTs).[4,14–18]

The mechanism of plasma polymerization tends to be a radical polymerization process,[19,20] especially when the plasma power is high. However, when the plasma power is low, the reaction tends to go through an ionic polymerization process.[21]

If the gas used during the plasma treatment is oxygen, for example, the plasma treatment will tend to generate oxygen-containing groups on the nanoparticle surface. However, if the gas is a monomer, then the plasma treatment will tend to deposit an ultrathin coating of the corresponding polymer onto the nanoparticles surface.

Correspondence to: L. F. Ramos-deValle (devalle@ciqa.mx).

Contract grant sponsor: CONACYT; contract grant number: 84424.

In this respect, Shi and He[4] were among the first to use this technique to treat carbon nanoparticles (CNT and CNF) while studying PC/CNT nanocomposites. Most recently, using the plasma polymerization technique on CNF, Ramos-deValle et al.[14] reported an increase of more than 100% on the tensile modulus of PS/CNF nanocomposites. They showed excellent adhesion obtained between the polymer and the CNF, which produced a telescoping effect on the nanofibers, when subjecting the nanocomposite to a tensile stress, suggesting that the strength of the interfacial adhesion was found to be superior to the forces that maintain the CNF graphitic layers together.

Polyamide 6 (PA6), an important commercial semicrystalline polymer, is widely used in engineering applications. Liu et al.[22] reported its crystalline structure to consist of alpha (α)- and gamma (γ)-phase crystals, of which the α-phase constituted the more stable phase. However, Phang et al.[23] reported that the favored formation of either the α- or γ-crystalline phase strongly depended on the cooling rate. Below 10°C/min, the α-crystalline phase would be favored, whereas above 10°C/min, the γ-crystalline phase would be favored. Other studies had found that the α-crystalline phase tended to be more rigid than the γ-phase.[24]

Concerning the use of nanoparticles, it has been found that nanoclay promotes the growth of the γ-crystalline phase of PA6 for both the melt-mixed and the *in situ* polymerized nanocomposites.[22,23,25–29] The total crystallinity and the fraction of the α- and γ-phases strongly depend on the nanoclay content and on the interactions between the PA6 and the nanoclay.

On the other hand, contrary to the effect of nanoclays, it has been found that CNTs promote the formation of the α-crystalline phase of PA6, independently of the rate of cooling.[22,23,30] This preferred formation of the α-phase could have an effect in producing a slightly higher modulus nanocomposite.[31–33]

The purpose of this work is to study the effect of plasma reactor parameters on the surface modification (surface coating) of CNF via plasma polymerization of acrylic acid and the effect of this modification on the compatibility between PA6 and CNF and on the properties of PA6/CNF composites.

EXPERIMENTAL

Materials

The polymer used was PA6 obtained from BASF America, Florham Park, NJ, with the trade name Ultramid B3, M_w of 60,000 and M_w/M_n of 2.4 and T_g and T_f of 60 and 220°C, respectively. Before use, PA6 was dried at 80°C for 20 h in a vacuum oven.

The CNFs were obtained from Applied Sciences, Dayton, OH, and are designated as Pyrograf III; these are 60–150 nm in diameter, 30–100 μm in length, and have a density of 1.95 g/cm^3 and a surface area of 55 m^2/g.

The acrylic acid used to modify the CNF, i.e., to produce an ultrathin poly(acrylic acid) (PAA) coating layer on the CNF, was obtained from Sigma-Aldrich, St. Louis, MO.

Methodology

Coating of the CNF via plasma polymerization

The CNFs were coated with an ultrathin PAA layer as acrylic acid monomer in the vapor phase was fed into and polymerized in the plasma reactor and deposited on the surface of the CNF.

Three different plasma polymerization conditions were tested: 50 W for 30 min (90 kJ), 100 W for 30 min (180 kJ), and 100 W for 60 min (360 kJ).

The plasma reactor consisted basically of a glass flask with a copper wire coiled around it and connected to a radio frequency generator. Details of this reactor were presented in a previous article.[14]

The process of plasma polymerization and deposition of PAA onto the CNF was carried out as follows: 1.5 g of CNF was introduced in the glass flask and put under vacuum. The initial system internal pressure was 0.3 Pa. Then, the acrylic acid monomer flow was fixed while the pressure was kept constant at 2.5 Pa. This pressure gave a constant acrylic acid gas flow, into the reactor, of 0.15 cm^3/min or of 1.5135×10^{-10} mol/min.

Dispersion of the untreated and treated CNF

The unmodified and modified nanofibers were tested for dispersion in water and ethanol as follows: 3 mg of the differently treated nanofibers were immersed into 10 mL of solvent and then agitated. After 10 min (which were designated as initially) and after 24 h, photographs were taken, and then the degree of dispersion, which indirectly indicates the degree of the CNF modification, was assessed.

Preparation of nanocomposites

All nanocomposites were prepared via melt-mixing in a Brabender torque rheometer mixing chamber, using cam-type rotors, at 240°C and 85 rpm for 15 min. In all cases, the 75-mL chamber was filled up to 93%, i.e., with 70 mL. The mixing procedure was as follows: the PA6 was introduced into the mixing chamber and the processing was started. Once the PA6 melted, the CNF were introduced during a period of 2 min. Thereafter, the mixing was continued for 13 more minutes to complete the 15-min mixing time. Finally,

the nanocomposites were extracted, grounded, compression molded at 230°C, and cooled down to room temperature at ca. 40°C/min (as if mildly quenched) to obtain 150 mm × 150 mm × 3 mm plates, from which tensile test specimens (ASTM D-638) were cutout.

Analysis of the nanocomposites (XRD, DSC, TGA, SEM, and tensile)

X-ray diffraction analysis was performed in a Siemens D5000 using Cu Kα X-ray radiation of 1.54 Å. The X-ray samples were obtained from the aforementioned compression moldings. The XRD patterns were scanned in the 2θ range from 10° to 60° at a rate of 0.6 θ/min, with an interval of 0.02° between two angle steps and an exposure time of 1 s for each step. The data obtained was smoothed with the Origin 7.0 Scientific Graphing and Data Analysis Software, obtained from OriginLab, Northhampton, England.

The thermal properties were evaluated in a MDSC-2920 (TA Instruments) as follows: the sample was first heated from 30 to 260°C at 10°C/min and kept at 260°C for 5 min, and then cooled down to 30°C at 10°C/min.

The thermogravimetric analysis was carried out in a MQ800 (TA Instruments) from 30 to 600°C at 10°C/min, under a nitrogen flow of 10 mL/min.

Fractured tensile specimens were studied through a Jeol JSM7401F scanning electron microscope (SEM) to assess the nanocomposite morphology and the "adhesion" between the CNF and the polymer matrix. To determine the thickness of the ultrathin PAA layer deposited on the CNF, the analysis was carried out via the scanning-transmission electron microscopy mode (STEM).

Tensile properties were measured on a United Tensile Tester 3M-10 machine, fitted with a 450 kg load cell at an extension rate of 5 mm/min. All tests were performed in accordance to ASTM D-638.

RESULTS AND DISCUSSION

Figure 1 shows two photographs of the vials containing the untreated and the plasma-treated CNF dispersed in water. It can clearly be observed that the untreated nanofibers remain suspended and agglomerated at the top, whereas the plasma-treated ones (treated with 50 W-30 min, 100 W-30 min, and 100 W-60 min), respectively, readily disperse and remain fairly dispersed after standing for 24 h. This suggests a change on the nanofibers from hydrophobic to hydrophilic because of the presence of the carboxyl acid groups in the ultrathin layer of PAA coating the nanofibers.

In addition, it is also observed that as the time of treatment in the plasma reactor increases, the dispersion of the CNF seems to be better and more stable, even after 24 h standing. The latter effect could be because of the longer the time of treatment, the more the CNF surface area is covered with PAA.

Figure 2 shows two photographs of the vials containing the untreated and treated CNF dispersed in ethanol. Similar effects as described earlier are observed. The untreated nanofibers precipitate and agglomerate at the bottom, whereas the plasma-treated ones are readily dispersed and remain fairly dispersed after standing for 24 h. Also, as the time of treatment increases, the dispersion of the CNF seems to be better and more stable, even after 24 h standing. These dispersability tests do not give a quantification of the degree of modification; however, they give a fair idea whether the modification on the CNF was achieved or not.

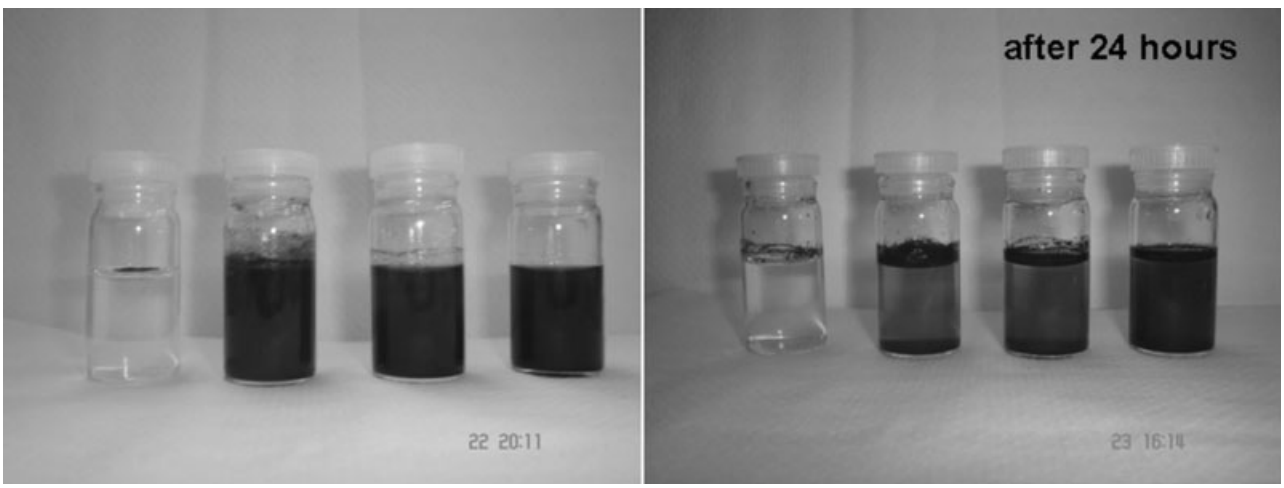

Figure 1 Dispersion of CNF in water. From left to right: untreated CNF, and treated CNF with 50 W-30 min, 100 W-30 min, and 100 W-60 min, respectively. Initially and after standing for 24 h.

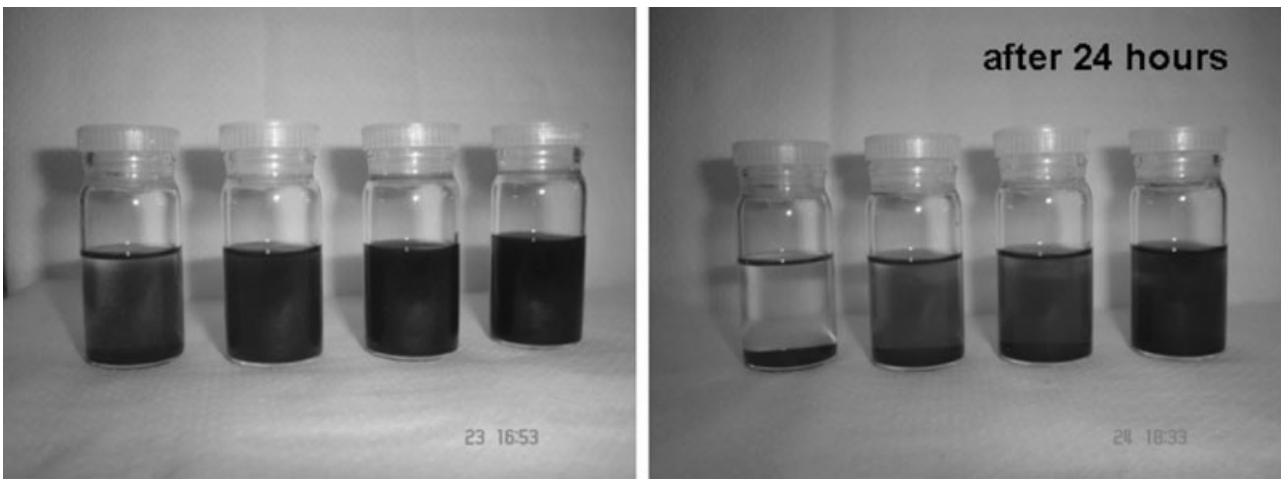

Figure 2 Dispersion of CNF in ethanol. From left to right: untreated CNF, and treated CNF with 50 W-30 min, 100 W-30 min, and 100 W-60 min, respectively. Initially and after standing for 24 h.

Figure 3, from FTIR analysis, shows unequivocally the formation of the PAA coating on the CNF surface as a result of the plasma treatment. The characteristic C—H, C=O, and C—O bands present in the PAA are observed.

Figure 4 shows the TGA results of pure and 50 W-30 min treated CNF. It can be observed that the weight loss of the treated CNF is greater than that of the untreated ones.

The weight loss of the treated CNF is up to 20% at 500°C, whereas the weight loss of the untreated CNF at 500°C is negligible. Considering that the PAA layer represents ca. 26% of the plasma-treated and coated CNF total volume, as explained later when discussing Figure 5, it is assumed that the weight loss of the treated CNF is entirely due to the decomposition of the PAA coating on the CNF.

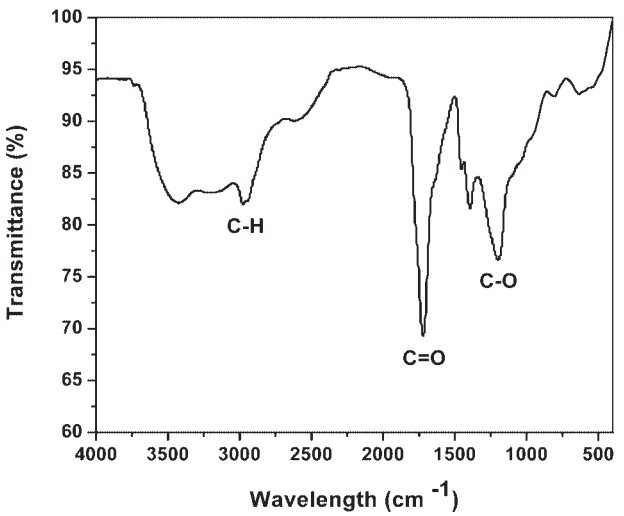

Figure 3 FTIR diagram of 50 W-30 min treated CNF, showing the characteristic bands due to the presence of the PAA coating.

Figure 5(A,B) shows the SEM micrographs of surface textures of the untreated and treated CNF. It can be observed that the untreated CNF present a smooth surface, whereas those treated with 100 W for 60 min present a rougher surface. This roughness is assumed to be due to the PAA coating deposited on the CNF after the plasma polymerization treatment. It is worth mentioning that the plasma polymerization affects only the CNF surface as indicated by some authors.[34] In addition, Figure 5(C,D) shows the micrographs obtained via STEM analysis of the untreated and treated CNF. Figure 5(C) shows the hollow structure of the CNF, and Figure 5(D) clearly shows a coating layer of $\sim$ 8 nm deposited on the CNF surface as a result of the plasma treatment. Also, from Figure 5(D), the internal and external diameters of the CNF can be estimated as $\sim$ 20 and $\sim$ 88 nm, respectively. Thus, considering the thickness of the PAA layer and the CNF dimensions, it

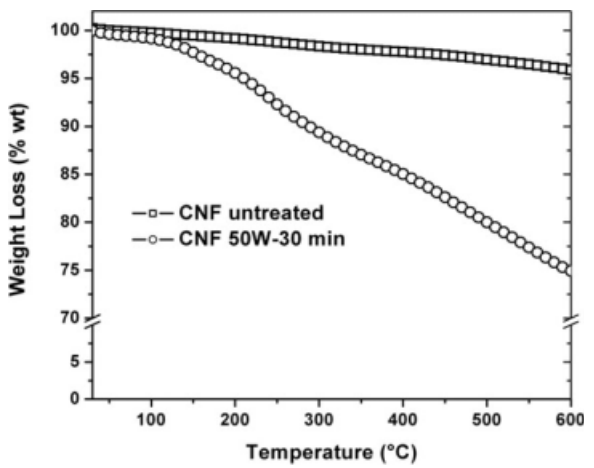

Figure 4 TGA results of pure and 50 W-30 min plasma-treated CNF.

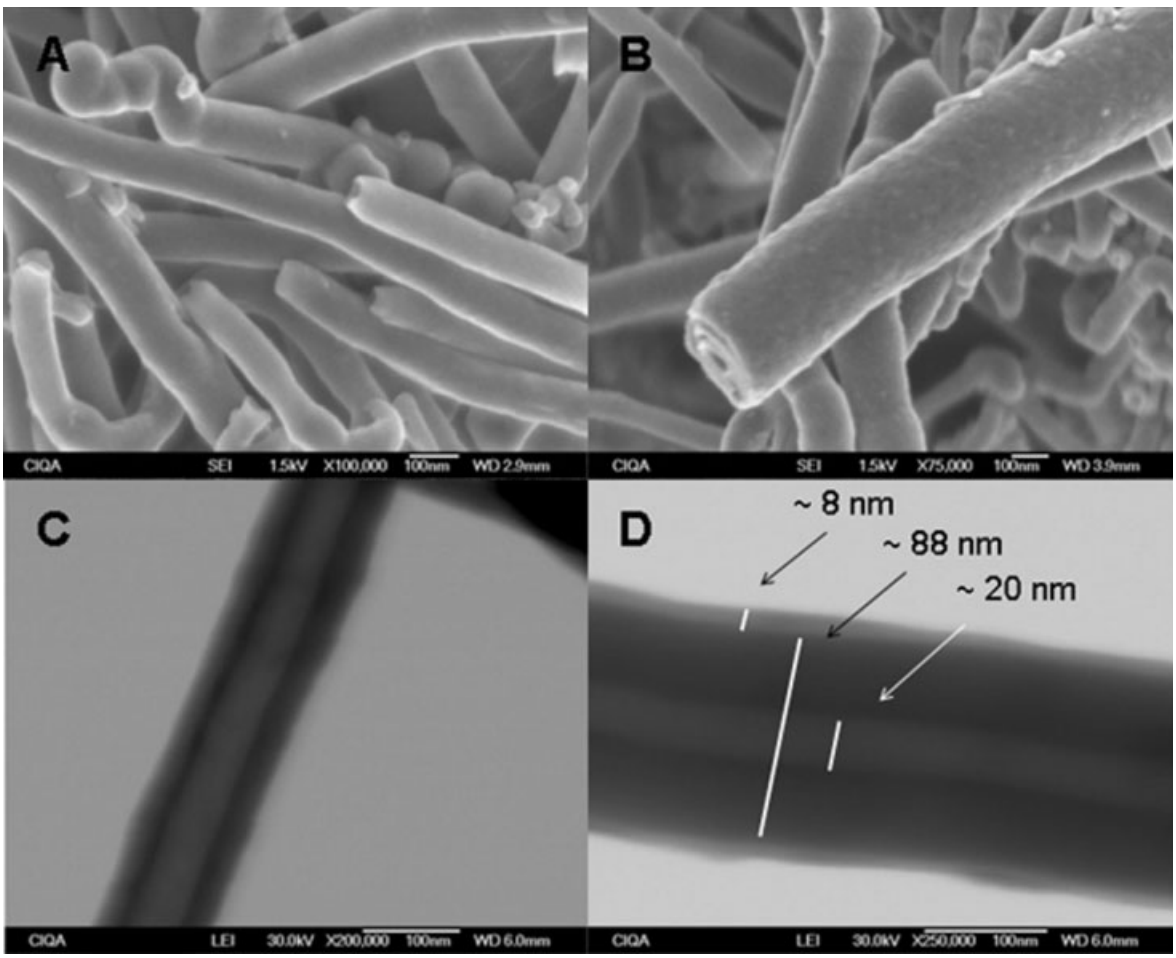

Figure 5 SEM micrographs of (A) untreated CNF and (B) plasma-treated CNF with 100 W for 60 min. STEM micrographs of (C) untreated CNF and (D) treated CNF with 50 W for 30 min.

can be estimated that the volume of the PAA layer represents ca. 26% of the whole plasma-treated CNF.

Figure 6 represents the SEM micrographs of the fractured surface of tensile specimens of PA6 and PA6/CNF nanocomposites. First, it is observed that pure PA6 [Fig. 6(A)] shows a ductile fracture, whereas the PA6 nanocomposites [Fig. 6(B–D)] presents a profile that appears to be more of a fragile fracture. With respect to the nanocomposites with treated CNF [Fig. 6(C,D)], the nanofibers dispersion appears to be much better and improved as the treatment goes from 50 W-30 min to 100 W-30 min.

Furthermore, Figure 6(D) shows some nanofibers that appear to be strongly adhered to the polymer matrix, which seem to be as inverted cones, as if pulling from above and forcing the nanofibers, strongly adhered to the polymer matrix on the outer layer, to tear and telescope in the inner layers. This result is attributed to the improved compatibility between the polymer matrix and the CNF because of the plasma treatment on the CNF.

Figure 7 shows the strong adhesion between the CNF and the polymer matrix. It appears that some nanofibers teared or telescoped instead of simply pulling out from the matrix because of the strong adhesion between the nanofibers and the polymer matrix.

Figure 8 shows the XRD patterns of PA6 and PA6/CNF nanocomposites. It is observed that pure PA6 presents the signals associated to both the α- and γ-crystalline structures. This coincides with the results reported by Phang et al.[23] for pure PA6, where it is shown that the favored formation of either the α- or γ-crystalline phase strongly depends on the cooling rate; the more rapid the cooling rate, the more formation of the γ-crystalline phase will be favored. In this respect, as mentioned in the "Experimental" section, the rate of cooling during the plates preparation via compression molding was ca. 40°C/min (mild quenching).

The XRD patterns of the PA6/CNF nanocomposites present only the signals that correspond to α-crystalline structure. This also coincides with reported results,[23,26] where it is shown that independently of the rate of cooling, the CNTs strongly favor the formation of the α-crystalline phase in PA6/CNT

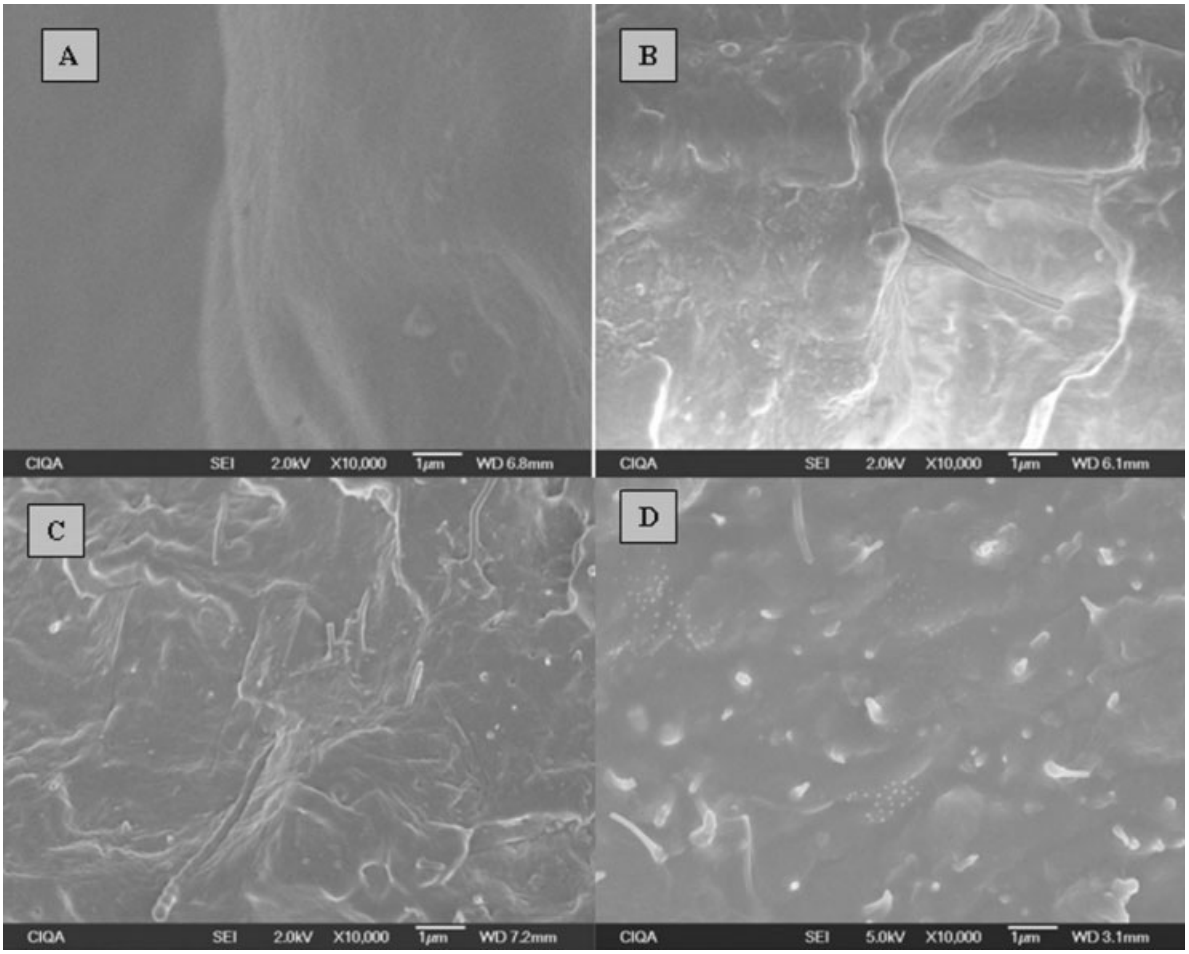

Figure 6 SEM micrographs of fractured tensile specimens of PA6 and PA6 nanocomposites: (A) pure PA6; (B) PA6/untreated CNF; (C) PA6/treated CNF 50 W-30 min; and (D) PA6/treated CNF 100 W-30 min. All micrographs are at ×10,000.

nanocomposites. This strongly suggests that CNF, like CNT, acts as an efficient nucleating agent, promoting the rapid formation of the α-crystalline phase.

The fusion thermograms, during heating of samples taken from the compression-molded plates, are shown in Figure 9. It can be observed that all thermograms are very similar among them. The fusion peak around 222°C suggests the sole presence of the α-crystalline phase in all samples, including the pure PA6 sample. This may be explained as follows: during heating at 10°C/min, the less stable γ-crystalline phase present in the pure PA6 sample, as observed in the XRD patterns of Figure 8, transforms into the more stable α-phase, so that only the fusion peak corresponding to the α-phase is observed.

However, after a thorough observation of the thermogram of the sample with treated CNF at 100 W-60 min, a very weak peak can be observed at 214°C, which indicates the presence of the γ-crystalline phase in very minute quantity.

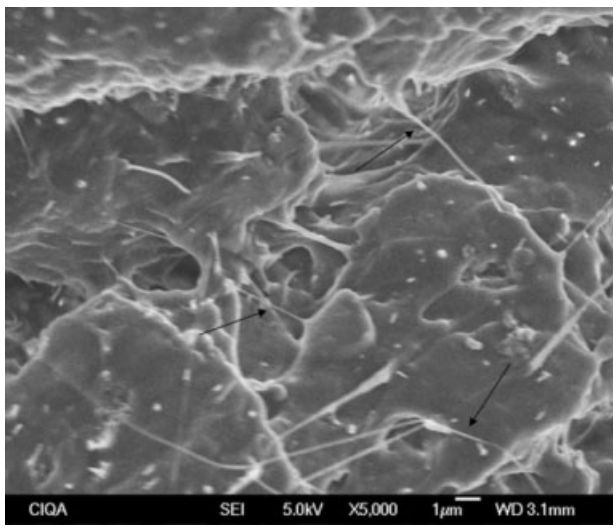

Figure 7 SEM micrograph of a fractured tensile specimen of PA6/treated CNF 100 W-30 min nanocomposite. The micrograph is at ×5000.

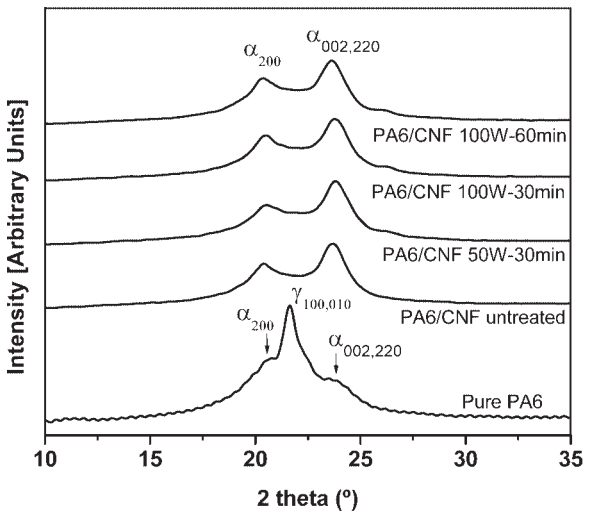

Figure 8 XRD patterns of pure PA6 and PA6/CNF nanocomposites.

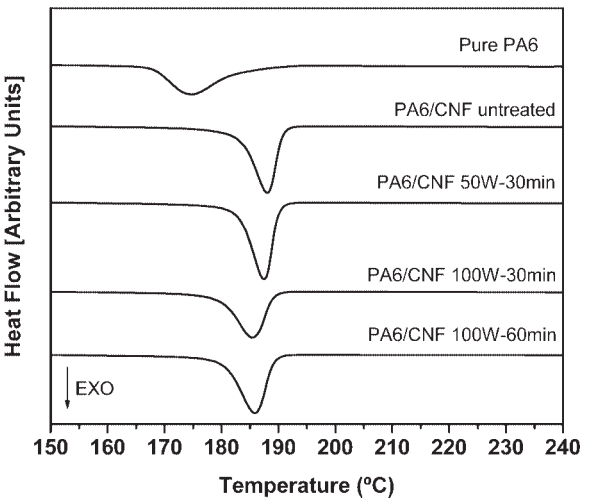

Figure 10 DSC crystallization thermograms of PA6 and PA6/CNF nanocomposites. Cooling at 10°C/min.

On the other hand, Figure 10 shows the crystallization thermograms of the same samples. The nucleating effect of the CNF can clearly be established. The crystallization peak of pure PA6 occurs at 175°C, whereas that of the nanocomposites occurs at 185–188°C. It is important to note that the crystallization peak goes from 188°C down to 185°C as the energy employed during the plasma treatment of the CNF goes from zero (untreated) to 360 kJ (100 W-60 min). It appears that the CNFs, at 3 wt %, increase the crystallization temperature of PA6 by 13°C, which demonstrates the efficiency of the CNF as nucleating agents. In fact, it has been reported that the CNF act slightly better as nucleating agents in PP than the CNT.[35]

In addition, it is observed that the crystallization peak goes from narrow to a bit wider as the energy employed during the plasma treatment of the CNF goes from 0 (untreated) to 360 kJ (100 W-60 min). Nonetheless, the crystallization peak is much wider for the pure PA6. These effects correspond to those produced by a good nucleating agent, which will produce smaller, more homogeneous crystalline phases, resulting in a narrower range of temperatures for crystallization.

Figure 11 shows the variation of tensile stress with deformation for PA6 and PA6 composites with 3 wt % of untreated and treated CNF.

It is observed that the addition of 3 wt % of CNF reduces the elongation at break, but increases the tensile stress of the nanocomposite. Also, it is observed that the elongation at break decreases and the modulus and tensile stress increase as the energy employed during the plasma treatment of the CNF

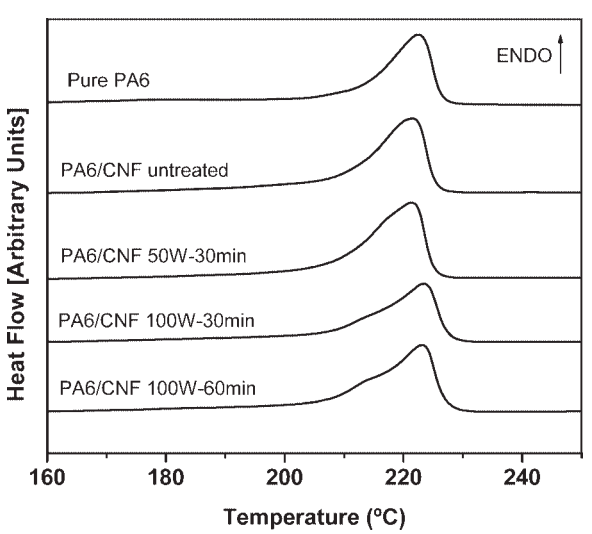

Figure 9 DSC fusion thermograms of PA6 and PA6/CNF nanocomposites. Heating at 10°C/min.

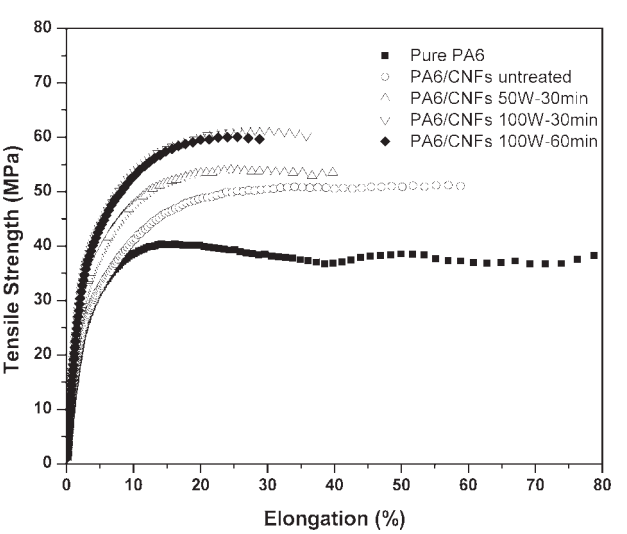

Figure 11 Tensile stress versus tensile strain of PA6 and PA6/CNF nanocomposites; all with 3 wt % CNF.

increases from 0 (untreated) to 360 kJ (100 W-60 min), that is, as the amount of the PAA layer deposited on the CNF increases. In this respect, it has been amply reported[36] that if there is adhesion (compatibility) between filler and polymer, there will be a restriction for the "stretching" of the sample due to the bonding between the polymer molecules and the rigid filler particles, that is, the tensile strength will increase, but the elongation will decrease. On the other hand, if there is no adhesion (no compatibility), there will be no restriction for the stretching, and the polymer molecules will slip and pass each other, that is, the tensile strength will decrease, but the elongation will also decrease (when compared with the pure polymer), although to a lesser extent.

In fact, as shown in Figure 12, the tensile stress increases by 30%, from 48 MPa (Sample B) to 62 MPa (Sample E), and the modulus increases by 48%, from 1140 MPa (Sample B) to 1680 MPa (Sample E), as the energy employed during the plasma treatment of the CNF increases from 0 (untreated) to 360 kJ (100 W-60 min). However, the increase in tensile stress and tensile modulus with respect to the pure PA6 (Sample E vs. Sample A) was 52 and 88%, respectively.

In this respect, the CNF may breakdown during processing that will decrease the CNF aspect ratio by about 20–80%. However, considering that the original CNF have an aspect ratio of 200–1000, this processing will diminish the aspect ratio down to 40–200, which anyhow, is enough to produce a reinforcing effect on the nanostructured polymer composite.

These results are clearly due to the improved compatibility and adhesion between the PAA-coated CNF and the polymer matrix, which permit the load transfer from the matrix to the nanofibers to occur more readily.

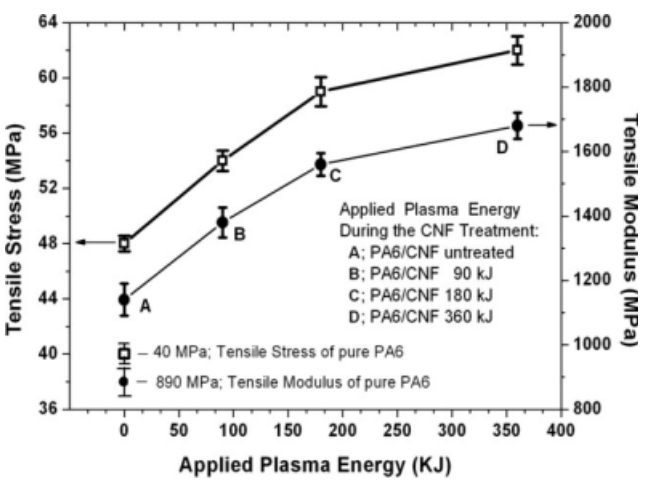

Figure 12 Variation of tensile stress and tensile modulus of PA6 and PA6/CNF nanocomposites with CNF content and treatment; all with 3 wt % CNF.

CONCLUSIONS

The ultrathin PAA coating deposited onto the CNF via plasma polymerization changed the distinct hydrophobic character of the CNF into hydrophilic.

This plasma treatment clearly helped to increase the compatibility and affinity of the CNF toward the PA6 polymer. The compatibility was exemplified in the SEM micrographs of the fractured nanocomposite tensile specimens, where the treated CNF appeared totally embedded in the PA6 matrix.

As a result of using untreated and treated CNF, the tensile stress and the tensile modulus increased by 30 and 48%, respectively. However, the increase in tensile stress and modulus with respect to pure PA6 was 52 and 88%, respectively.

Treated CNF markedly increased tensile properties.

Treated CNF also acted as a nucleating agent, specifically in promoting the formation of the α-crystalline phase, shifting the crystallization temperature of PA6 by 13°C from 175 to 188°C.

One of the authors, E.H.H., thank CONACYT for a scholarship to carry out his PhD studies. Finally, the authors also wish to thank E. Saucedo-Salazar, M. L. López-Quintanilla, M. G. Méndez-Padilla, B. M. Huerta-Martínez, S. Tórres-Rincón, M. C. Gonzalez-Cantu, J. Rodriguez-Velazquez, J. F. Zendejo, A. Cardenas-Quinones, H. Prado-Lopez, and E. Hurtado-Suarez for their support in the nanocomposites preparation and characterization, as well as in the preparation of figures.

References

1. Qu, L. V.; Veca, L. M.; Lin, Y.; Kitaygorodsky, A.; Chen, B.; McCall, A. M.; Connel, J. W.; Sun, Y. P. Macromolecules 2005, 38, 10328.
2. Hill, D.; Lin, Y.; Qu, L.; Kitaygorodskiy, A.; Connell, J. W.; Allard, L. F.; Sun, Y. P. Macromolecules 2005, 38, 7670.
3. Ros, T. G.; van Dillen, A. J.; Geus, J. W.; Kiningsberger, D. C. Chem Eur J 2002, 8, 1151.
4. Shi, D.; He, P. Rev Adv Mater Sci 2004, 7, 97.
5. Park, S. H.; Kim, S. D. Polym Bull 1994, 33, 249.
6. Inagaki, N.; Tasaka, S.; Ishii, K. J Appl Polym Sci 1993, 48, 1433.
7. Yoshida, K.; Greener, E. H. J Dentistry 1994, 22, 57.
8. Wang, M.; Bonfield, W. Biomaterials 2001, 22, 1311.
9. Shang, X. Y.; Zhu, Z. K.; Yin, J.; Ma, X. D. Chem Mater 2002, 14, 71.
10. Xu, M.; Zhang, T.; Gu, B.; Wu, J.; Chen, Q. Macromolecules 2006, 39, 3540.
11. Lozano, K.; Barrera, E. V. J Appl Polym Sci 2001, 79, 125.
12. Westerdahl, C. A. L.; Hall, J. R.; Schramm, E. C.; Levi, D. W. J Colloid Interface Sci 1974, 47, 610.
13. Kogoma, M.; Kasai, H.; Takahashi, K.; Moriwaki, T.; Olazaki, S. J Phys D: Appl Phys 1987, 20, 147.
14. Ramos-deValle, L. F.; Neira-Velázquez, M. G.; Hernández-Hernández, E. J Appl Polym Sci 2008, 107, 1893.
15. Harper-Nixon, D. W. Abstr Am Chem Soc 2002, 224, U299.
16. Weinkauf, D. H.;Harper-Nixon, D.; Wyatt, J.; Jeon, H. S. Abstr Am Chem Soc 2002, 224, U619.
17. Shi, D.; Hee, P.; Lian, J.; Wang, L. M.; Ooij, W. J Mater Res 2002, 17, 2555.

18. Shi, D.; Wang, S. X.; van Ooij, W. J.; Wang, L. M.; Zhao, J.; Yu, Z. Appl Phys Lett 2001, 78, 1243.
19. Schulze, R. D.; Friedrich, J. F.2nd Workshop on Self Excited Electron Plasma Resonance Spectroscopy, Dresden, Germany, December 2000.
20. Yasuda, H.Plasma Polymerization; Academic Press: London, 1985.
21. Orhan, B. Ö.; Hacaloğlu, J.; Akovali, G. Eur Polym J 1991, 27, 1405.
22. Liu, T.; Tjiu, W. C.; He, C.; Na, S. S.; Chung, T. S. Polym Int 2004, 53, 392.
23. Phang, I. Y.; Ma, J.; Shen, L.; Liu, T.; Zhang, W. D. Polym Int 2006, 55, 71.
24. Ito, M.; Mizuochi, K.; Kanamoto, T. Polymer 1998, 39, 4593.
25. Lincoln, D. M.; Vaia, R. A.; Wang, Z.-G.; Hsiao, B. S. Polymer 2001, 42, 1621.
26. Liu, T. X.; Liu, Z. H.; Ma, K. X.; Shen, L.; Zeng, K. Y.; He, C. B. Compos Sci Technol 2003, 63, 331.
27. Lincoln, D. M.; Vaia, R. A.; Wang, Z. G.; Hsiao, B. S.; Krishnamoorti, R. Polymer 2001, 42, 9975.
28. Medellín-Rodriguez, F. J.; Burger, C.; Hsiao, B. S.; Chu, B.; Vaia, R. A.; Phillips, S. Polymer 2001, 42, 9015.
29. Lincoln, D. M.; Vaia, R. A.; Krishnamoorti, R. Macromolecules 2004, 37, 4554.
30. Liu, T.; Phang, I. Y.; Shen, L.; Chow, S. Y.; Zhang, W. D. Macromolecules 2004, 37, 7214.
31. Zhang, W. D.; Shen, L.; Phang, I. Y.; Liu, T. Macromolecules 2004, 37, 256.
32. Larios-López, L. L.MSc Thesis, Universidad Autónoma de San Luis Potosí, México, 1997.
33. Medellin-Rodriguez, F. J.; Larios-López, L.; Zapata-Espinoza, A.; Dávalos-Montoya, O.; Phillips, P. J.; Lin, J. S. Macromolecules 2004, 37, 1799.
34. Brandl, W.; Marginean, G. Proceedings of the 30th International Conference on Metallurgical Coatings and Thin Films; Elsevier: New York, 2004; p 181–186.
35. Reyes-deVaaben, S.; Aguilar., A.; Avalos, F.; Ramos-deValle, L. F. J Therm Anal Cal 2008, 93, 947.
36. Wypych, G.In Handbook of Fillers; ChemTech Publishing: Toronto, Canada, 2000; Chapter 8.